

000 001 002 003 004 005 LEARNING INTER-ATOMIC POTENTIALS WITHOUT 006 EXPLICIT EQUIVARIANCE 007 008 009

010 **Anonymous authors**
011
012
013
014
015
016
017
018
019
020
021
022
023
024
025
026
027
028

029 Paper under double-blind review
030
031

032 ABSTRACT

033 Accurate and scalable machine-learned inter-atomic potentials (MLIPs) are es-
034 sential for molecular simulations ranging from drug discovery to new material
035 design. Current state-of-the-art models enforce roto-translational symmetries
036 through equivariant neural network architectures, a hard-wired inductive bias
037 that can often lead to reduced flexibility, computational efficiency, and scal-
038 ability. In this work, we introduce **TransIP**: **T**ransformer-based **I**nter-**A**tomic
039 **P**otentials, a novel training paradigm for interatomic potentials achieving sym-
040 metry compliance without explicit architectural constraints. Our approach guides
041 a generic non-equivariant Transformer-based model to learn $SO(3)$ -equivariance
042 by optimizing its representations in the embedding space. Trained on the recent
043 Open Molecules (OMol25) collection, a large and diverse molecular dataset built
044 specifically for MLIPs and covering different types of molecules (including small
045 organics, biomolecular fragments, and electrolyte-like species), TransIP attains
046 comparable performance in machine-learning force fields versus state-of-the-art
047 equivariant baselines. Further, compared to a data augmentation baseline, TransIP
048 achieves 40% to 60% improvement in performance across varying OMol25
049 dataset sizes. More broadly, our work shows that learned equivariance can be
050 a powerful and efficient alternative to equivariant or augmentation-based MLIP
051 models.
052

053 1 INTRODUCTION

054 Atomistic simulations are a fundamental task in chemistry and materials science (Zhang et al., 2018;
055 Deringer et al., 2019), with Density Functional Theory (DFT) serving as a basis for accurately
056 calculating interatomic forces and energies. However, the utility of DFT is severely restricted by
057 its computational costs, which typically scale cubically with system size, rendering large-scale or
058 long-timescale simulations intractable. This has motivated machine-learned interatomic potentials
059 (MLIPs) to overcome this limitation by learning the potential energy surface from data, offering
060 orders-of-magnitude speed-ups compared to DFT calculations (Noé et al., 2020; Batzner et al., 2022;
061 Batatia et al., 2022; Jacobs et al., 2025; Leimeroth et al., 2025).

062 Equivariant neural networks have become a central paradigm for MLIPs due to their ability to encode
063 the three-dimensional structure of molecular graphs (Anderson et al., 2019; Thölke & Fabritiis,
064 2022; Liao et al., 2024a; Fu et al., 2025). These architectures are designed to explicitly respect roto-
065 translational symmetries ($SE(3)$ equivariance) by construction, often employing compute-intensive
066 mechanisms like spherical harmonics or equivariant message passing (Fuchs et al., 2020; Passaro &
067 Zitnick, 2023a; Liao & Smidt, 2023; Maruf et al., 2025). However, due to the design difficulties and
068 limited expressive power of these architectures (Joshi et al., 2023; Cen et al., 2024), a recent trend
069 in predictive and generative modeling is to use unconstrained models when enough data is available
070 (Wang et al., 2024; Abramson et al., 2024; Zhang et al., 2025a; Joshi et al., 2025).

071 In this paper, we introduce **TransIP** (**T**ransformer-based **I**nteratomic **P**otentials), a training
072 paradigm that achieves molecular symmetry for interatomic potentials *without* imposing architec-
073 tural $SO(3)$ constraints. TransIP steers a standard transformer toward $SO(3)$ equivariance via an
074 additional contrastive objective, allowing the model to retain the scalability and hardware efficiency
075 of attention mechanisms while learning symmetry from data.
076

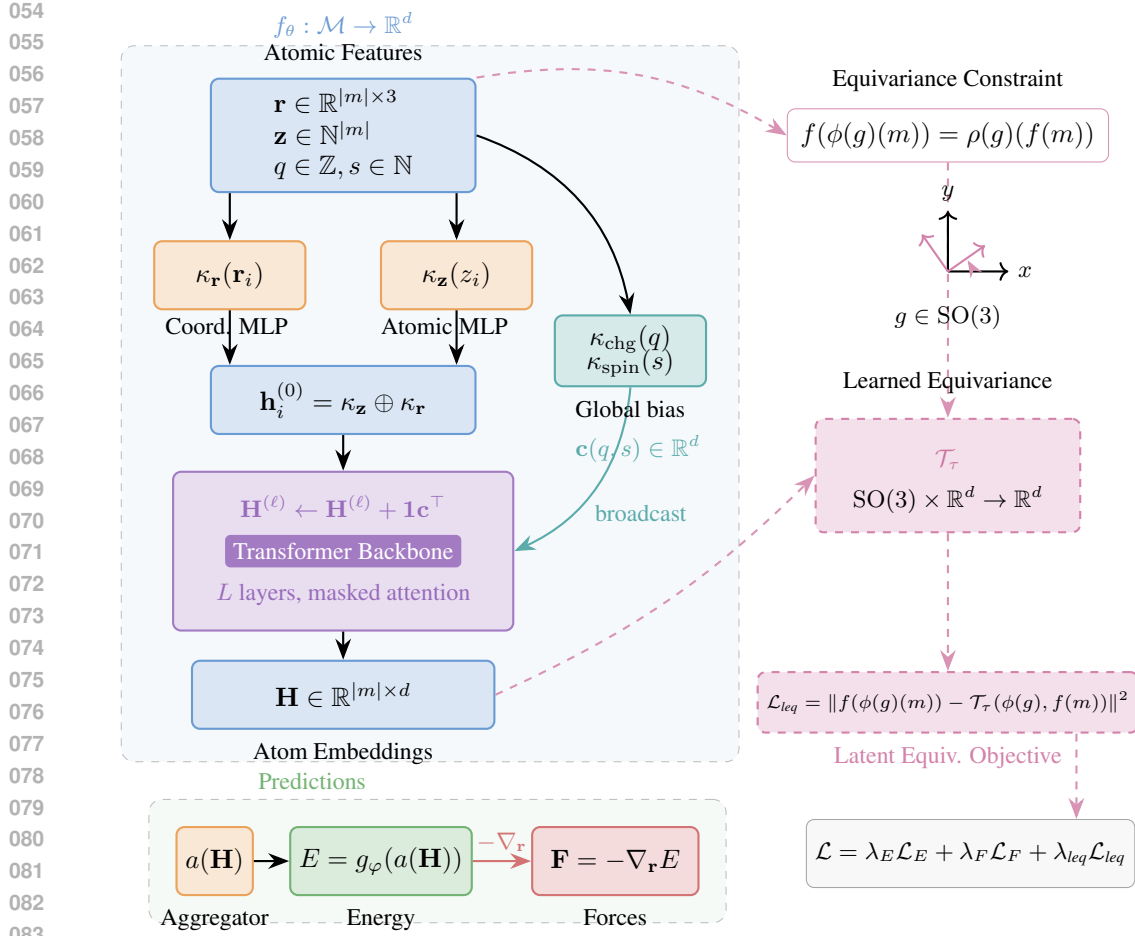


Figure 1: TransIP: Transformer-based Interatomic Potentials.

Our contributions are as follows:

- We propose an MLIP training pipeline with a general transformer-based model to obtain $\text{SO}(3)$ equivariance through training rather than hard-wired equivariant layers.
- We introduce an architecture-agnostic contrastive loss function that promotes $\text{SO}(3)$ equivariance in the embedding space of an unconstrained model. By aligning latent features across $\text{SO}(3)$ transformations in the model’s backbone, we show that TransIP scales better across different datasets and model sizes compared to traditional data augmentation techniques.
- On a diverse molecular benchmark, Open Molecules 25 (Levine et al., 2025) (that includes small organics, biomolecular fragments, electrolyte-like species), we show that TransIP outperforms data augmentation techniques and achieves comparable performance versus current state-of-the-art MLIP baselines.

2 SYMMETRY IN EMBEDDING SPACE

2.1 PROBLEM FORMULATION

Molecular representations. Let \mathcal{M} denote the space of molecular configurations. Each molecule $m \in \mathcal{M}$ is represented by atomic features $\mathbf{x} = (\mathbf{r}, \mathbf{z}, q, s)$, where $\mathbf{r} \in \mathbb{R}^{|m| \times 3}$ are atomic coordinates, $\mathbf{z} \in \mathbb{N}^{|m|}$ are atomic numbers, $q \in \mathbb{Z}$ is the total molecular charge, and $s \in \mathbb{N}$ is the spin multiplicity, with $|m|$ denoting the number of atoms in molecule m .

108 Our goal is to learn an embedding function $f_\theta : \mathcal{M} \rightarrow \mathbb{R}^d$ that maps molecular configurations to
 109 a d -dimensional latent space, and a prediction function $g_\varphi : \mathbb{R}^d \rightarrow \mathbb{R}$ that acts in the embedding
 110 space \mathbb{R}^d and outputs molecular properties (e.g., energy). Both f_θ and g_φ are neural networks
 111 parameterized by θ and φ , respectively.

112 **Symmetry groups.** We define a symmetry group G that acts on a set \mathcal{X} as a group of bijective
 113 functions from \mathcal{X} to itself, and the group operation is function composition. We say a function f is
 114 *equivariant* w.r.t. the group G if for every transformation $g \in G$ and every input $x \in X$,

$$116 \quad f(\phi(g)(x)) = \rho(g)(f(x)) \quad (1)$$

118 The group representations ϕ and ρ specify how we apply the elements of the group G on input
 119 and output data. As a concrete case, we can define G as a rotation group $\text{SO}(3)$ over molecular
 120 configurations \mathcal{M} , with $g \in \text{SO}(3)$ representing an element of G that acts on a molecule m by
 121 rotating the coordinates of each atom in 3D space. Formally, for a molecule $m = (\mathbf{r}, \mathbf{z}, q, s)$ with
 122 coordinates $\mathbf{r} = (\mathbf{r}_1, \dots, \mathbf{r}_{|m|})$, $\mathbf{r}_i \in \mathbb{R}^3$, the input action rotates each atom:

$$123 \quad (\phi(g) m) = ((R\mathbf{r}_1, \dots, R\mathbf{r}_{|m|}), \mathbf{z}, q, s).$$

125 Here R is a 3×3 rotation matrix (orthogonal with $\det R = 1$); \mathbf{z}, q, s are unchanged. An asso-
 126 ciated output representation rotates vector-valued quantities—e.g., for forces $\mathbf{F} = (\mathbf{F}_1, \dots, \mathbf{F}_{|m|})$,
 127 $\rho(g)\mathbf{F} = (R\mathbf{F}_1, \dots, R\mathbf{F}_{|m|})$ —while scalar outputs such as energies remain invariant, $\rho(g)E = E$.

128 2.2 IMPLICIT EQUIVARIANCE IN EMBEDDING SPACE

130 We seek an embedding function f that behaves equivariantly with respect to the symmetry group G ,
 131 meaning there exists a transformation $\rho(g) : \mathbb{R}^d \rightarrow \mathbb{R}^d$ such that:

$$133 \quad f(\phi(g)(m)) = \rho(g)(f(m)) \quad \forall g \in G, m \in \mathcal{M} \quad (2)$$

135 Common approaches enforce equivariance constraints through specialized architectures. Instead,
 136 we want the embedding function f to learn symmetry without equivariance constraints. However,
 137 with G being the rotation group $\text{SO}(3)$ on \mathcal{M} and the output of f being a high-dimensional vector,
 138 there is no direct representation of $\rho(g)$ to act in the space of \mathbb{R}^d . Thus, rather than specifying
 139 $\rho(g)$ analytically, we propose to learn the group transformation on an embedding vector in \mathbb{R}^d using
 140 a neural network $\mathcal{T}_\tau : \text{SO}(3) \times \mathbb{R}^d \rightarrow \mathbb{R}^d$ parameterized by τ . \mathcal{T} can be understood as a non-
 141 linear function that learns the group action implicitly on a latent vector, by providing the group
 142 representation on the input data.

143 3 LEARNING INTER-ATOMIC POTENTIALS WITHOUT EXPLICIT 144 EQUIVARIANCE

147 In this section, we introduce our training framework: TransIP (Transformer-based Inter-atomic Po-
 148 tentials), a new approach that achieves $\text{SO}(3)$ -equivariance through learned transformations in an
 149 embedding space without explicit equivariance constraints. Our method, illustrated in Figure 1, con-
 150 sists of three key components: (i) an unconstrained Transformer backbone that processes molecular
 151 configurations, (ii) a learned transformation network that performs group actions in the embedding
 152 space, and (iii) a contrastive objective that enforces latent equivariance (equiv.) during training.

153 3.1 TRANSIP: TRANSFORMER-BASED INTERATOMIC POTENTIALS

155 **Atom as tokens.** We model each molecule as a variable-length sequence of tokens, where each
 156 token represents an atom. Unlike conventional graph neural networks that construct edges based on
 157 distance cutoffs or neighbours’ atoms, we process all atoms within a molecule through self-attention,
 158 bounded by a maximum context length N_{ctx} . For batch processing, we use padding masks to prevent
 159 cross-molecule attention, ensuring each molecule is processed independently.

160 In addition, we apply rotary position embeddings (RoPE) (Su et al., 2023) to the queries $\mathbf{q}_i \in \mathbb{R}^{d/h}$
 161 and keys $\mathbf{k}_j \in \mathbb{R}^{d/h}$ of each attention head, where i, j denote the sequence positions of atoms within

162 a molecule, d is the model dimension, and h is the number of attention heads. The attention weights
 163 are computed as:

$$165 \quad \tilde{\mathbf{q}}_i = \text{RoPE}(\mathbf{q}_i, i), \quad \tilde{\mathbf{k}}_j = \text{RoPE}(\mathbf{k}_j, j) \\ 166 \quad \alpha_{ij} = \text{softmax} \left(\frac{\tilde{\mathbf{q}}_i^\top \tilde{\mathbf{k}}_j}{\sqrt{d/h}} + m_{ij} \right) \\ 168$$

170 where $\text{RoPE}(\cdot, \cdot)$ is the rotary position encoding operator, and $m_{ij} \in \{0, -\infty\}$ is the attention mask
 171 that blocks padding tokens and enforces within-molecule attention. This approach eliminates the
 172 need for explicit distance cutoffs while maintaining flexibility in modeling molecular interactions.

173 **Transformer Backbone.** We implement the embedding function $f_\theta : \mathcal{M} \rightarrow \mathbb{R}^d$ as a Transformer
 174 encoder that processes atom-level tokens. Each atom i is initialized with a token representation:

$$176 \quad \mathbf{h}_i^{(0)} = \kappa_{\mathbf{z}}(z_i) \oplus \kappa_{\mathbf{r}}(\mathbf{r}_i) \\ 177$$

178 where $\kappa_{\mathbf{z}} : \mathbb{N} \rightarrow \mathbb{R}^d$ and $\kappa_{\mathbf{r}} : \mathbb{R}^3 \rightarrow \mathbb{R}^d$ are learnable MLPs that embed atomic numbers and centered
 179 coordinates (with $\mathbf{r}_i \leftarrow \mathbf{r}_i - \frac{1}{|m|} \sum_j \mathbf{r}_j$), and \oplus denotes concatenation. These tokens are processed
 180 through L Transformer layers with masked self-attention within each molecule, producing final per-
 181 atom embeddings $\mathbf{H} = [\mathbf{h}_1, \dots, \mathbf{h}_{|m|}]^\top \in \mathbb{R}^{|m| \times d}$.

182 **Global Molecular Properties.** Following Levine et al. (2025), we incorporate global molecular
 183 properties (total charge q and spin multiplicity s of a molecule m) through learnable embeddings,
 184 and form a graph-level bias:

$$185 \quad \mathbf{c}(q, s) = \kappa_{\text{chg}}(q) + \kappa_{\text{spin}}(s) \in \mathbb{R}^d \\ 186$$

187 where κ_{chg} and κ_{spin} are learnable embedding functions for charge and spin, respectively. This
 188 global bias is broadcast-added at each Transformer layer: $\mathbf{H}^{(\ell)} \leftarrow \mathbf{H}^{(\ell)} + \mathbf{1}\mathbf{c}(q, s)^\top$.

189 **Energy and Force Predictions.** For molecular property prediction, we employ a permutation-
 190 invariant aggregator $a : \mathbb{R}^{|m| \times d} \rightarrow \mathbb{R}^d$ followed by an energy prediction head $g_\varphi : \mathbb{R}^d \rightarrow \mathbb{R}$:

$$192 \quad E_\varphi(m) = g_\varphi(a(\mathbf{H})) \\ 193$$

194 Forces are computed as conservative gradients of the energy with respect to atomic positions:

$$196 \quad \mathbf{F}(m) = -\nabla_{\mathbf{r}} E_\varphi(m) \in \mathbb{R}^{|m| \times 3} \\ 197$$

198 3.2 LEARNED LATENT EQUIVARIANCE

200 **Transformation Network.** We propose a transformation network $\mathcal{T}_\tau : \text{SO}(3) \times \mathbb{R}^d \rightarrow \mathbb{R}^d$ that
 201 learns how group actions (e.g., rotations) act on molecular embeddings. We implement \mathcal{T}_τ as a
 202 multilayer perceptron that takes as input the group representation in the input domain $\phi(g)$ and the
 203 molecular embedding $f(m)$. Formally,

$$204 \quad \mathcal{T}_\tau(\phi(g), f(m)) = \text{MLP}_\tau([\phi(g), f(m)]) \\ 205$$

206 where $[\cdot, \cdot]$ denotes concatenation and MLP_τ is a multilayer perceptron with parameters τ .

208 **Contrastive Objective for Latent Equivariance:** To learn the molecular symmetry without archi-
 209 tectural constraints, we define our latent equivariance loss as:

$$210 \quad \mathcal{L}_{\text{leq}}(\phi(g), m, f, \mathcal{T}) = \|f(\phi(g)(m)) - \mathcal{T}_\tau(\phi(g), f(m))\|^2 \quad (3) \\ 211$$

212 This loss encourages the embedding function f to behave equivariantly with respect to the symmetry
 213 group G , as mediated by the transformation network \mathcal{T}_τ . During training, we sample a molecule m
 214 from the dataset and a rotation element g uniformly from $\text{SO}(3)$ and minimize the expected latent
 215 loss:

$$216 \quad \min \mathbb{E}_{m \sim \mathcal{M}, g \sim \text{SO}(3)} [\mathcal{L}_{\text{leq}}(\phi(g), m, f, \mathcal{T})] \quad (4)$$

216 3.3 TRAINING OBJECTIVE
217218 Our training objective combines three complementary losses for accurate prediction of energy and
219 forces as well as implicitly learning molecular symmetry.
220221 **Prediction Losses.** For energy and force predictions, we use:
222

223
$$\mathcal{L}_E = \frac{1}{|m|} |E_\varphi(m) - E^*| \quad (\text{per-atom mean absolute error (MAE)}) \quad (5)$$

224
$$\mathcal{L}_F = \frac{1}{3|m|} \|\mathbf{F}(m) - \mathbf{F}^*\|_F^2 \quad (\text{per-molecule mean squared error (MSE)}) \quad (6)$$

225 where E^* and \mathbf{F}^* are ground-truth energies and forces, and $\|\cdot\|_F$ denotes the Frobenius norm. For
226 energies, we use referenced targets as described by Levine et al. (2025).
227228 **Combined Objective.** Training combines three weighted terms: (i) the latent equivariance target
229 \mathcal{L}_{leq} defined in Eq. 3; (ii) energy loss \mathcal{L}_E ; and (iii) force loss \mathcal{L}_F . The total objective is
230

231
$$\mathcal{L}_{\text{total}} = \lambda_E \mathcal{L}_E + \lambda_F \mathcal{L}_F + \lambda_{leq} \mathcal{L}_{leq} \quad (7)$$

232

233 where λ_E , λ_F , and λ_{leq} are hyperparameters for each loss. The optimal hyperparameters are given
234 in Table 5 of Appendix A.
235236 4 RELATED WORK
237238 **ML Interatomic Potentials.** Using machine learning (ML) methods to predict energies and forces
239 of different molecular systems and materials has been an active area of research (Schütt et al., 2017;
240 Chmiela et al., 2022; Musaelian et al., 2023; Liao et al., 2024b; Yang et al., 2025). Due to the
241 intricate 3D structures of atomistic systems, equivariant designs such as steerable convolution (Co-
242 hen & Welling, 2017; Brandstetter et al., 2022) and higher-order tensors (Thomas et al., 2018), as
243 well as covariant representation (Anderson et al., 2019), have been essential backbones for mod-
244 eling molecular systems. For example, Gasteiger et al. (2020); Klicpera et al. (2021) introduced
245 equivariant directional message passing between pairs of atoms with a spherical harmonics repre-
246 sentation. In contrast, Batzner et al. (2022) developed equivariant convolution with tensor-products
247 and Batatia et al. (2022) built higher-order messages with equivariant graph neural networks (Sator-
248 ras et al., 2021). Additionally, Passaro & Zitnick (2023b) reduced the computational complexity of
249 SO(3) convolution and replaced it with SO(2) convolutions, which have been used as a backbone
250 for MLIPs (Fu et al., 2025). More recently, Rhodes et al. (2025) presented Orb-v3 models with
251 improved computational efficiency, built on Graph Network Simulators (Sanchez-Gonzalez et al.,
252 2020).
253254 **Unconstrained ML models.** While current-state-of-the-art MLIP models primarily rely on equiv-
255 ariant GNNs, unconstrained models are actively used in other domains. For example, integrating
256 data augmentation via image transformations has been used in different vision tasks, from classi-
257 fication (Inoue, 2018; Dosovitskiy et al., 2021; Rahat et al., 2024) to segmentation (Negassi et al.,
258 2022; Yu et al., 2023). For geometric data, the use of unconstrained models and diffusion Trans-
259 formers (without explicit equivariance constraints) has been a recent trend in generative tasks, e.g.,
260 AlphaFold 3 for biomolecular structure prediction (Abramson et al., 2024) as well as molecular
261 conformation and materials generation (Wang et al., 2024; Zhang et al., 2025a; Joshi et al., 2025).
262 In contrast, several works have been introduced to overcome the limitations of strictly equivariant
263 GNNs by enforcing symmetry via frame averaging over geometric inputs (Puny et al., 2022; Duval
264 et al., 2023; Lin et al., 2024; Huang et al., 2024; Dym et al., 2024); learning canonicalization func-
265 tions that map inputs to a canonical orientation before prediction (Kaba et al., 2022; Baker et al.,
266 2024; Ma et al., 2024; Lippmann et al., 2025); or learning equivariance through data augmentation
267 with molecule-specific graph-based architectures (Qu & Krishnapriyan, 2024; Mazitov et al., 2025).
268 However, in this work, we demonstrate that an unconstrained general-purpose Transformer model
269 can serve as a backbone for MLIPs, which replaces graph-based inductive biases with a scalable
latent equivariance objective that implicitly learns equivariant features without explicit equivariance
constraints.

270 5 EXPERIMENTAL SETUP
271

272 **Dataset.** We train and evaluate our proposed method **TransIP** on the Open Molecules 2025
273 (OMol25) collection (Levine et al., 2025), a large-scale molecular DFT dataset for ML interatomic
274 potentials. OMol25 covers 83 atomic elements and diverse chemistries including: metal complexes,
275 electrolytes, biomolecules, SPICE, neutral organic, and reactivity. It contains molecules from sev-
276 eral datasets such as ANI-2X (Devereux et al., 2020), Transition-1X (Schreiner et al., 2022), ANI-
277 1xBB (Zhang et al., 2025b), Orbnet Denali (Christensen et al., 2021), SPICE2 (Eastman et al., 2022;
278 2024), and Solvated Protein Fragments (Unke & Meuwly, 2019). Following Levine et al. (2025),
279 we use the official 4M training split (3,986,754) and the out-of-distribution composition validation
280 split *Val-Comp* (2,762,021). *Val-Comp* consists of molecules gathered from various datasets and
281 domains, such as biomolecules, neutral organics, and metal complexes.

282 **Model Configurations.** We evaluate TransIP across three model scales: Small (14M parameters),
283 Medium (85M parameters), and Large (302M parameters). All models use MLP-based coordinate
284 embeddings and RoPE positional encodings. The transformation network \mathcal{T}_τ is a 2-layer MLP with
285 GELU activations and 2d hidden dimension.

286 **Training Setup.** Using the standardized FAIRCHEM Python package (Shuaibi et al., 2025), we train
287 TransIP on the OMol25 dataset using an AdamW optimizer with learning rate 5×10^{-4} , weight
288 decay 10^{-3} , and gradient norm clipping at 200. We use a cosine learning rate schedule with linear
289 warmup over the first 1% of training, followed by cosine decay down to 1% of the initial lr. The
290 loss weights are set to $\lambda_E = 5$ for energies and $\lambda_F = 15$ for forces. For the latent equivariance
291 objective λ_{leg} , we sweep the values in $\{1, 5, 10, 100\}$ and selected $\lambda_{leg} = 5$ based on validation
292 performance.

293 **Scalability Experiments.** We conduct three sets of experiments to assess TransIP’s scaling behav-
294 ior:

- 295 • **Data scaling:** We train the Small (14M parameter) model on three dataset sizes (1M, 2M,
296 4M molecules) for 5 epochs using 8 NVIDIA 80GB GPUs, comparing TransIP with learned
297 equivariance against an unconstrained Transformer version with SO(3) data augmentation
298 (TransAug).
- 300 • **Model size scaling.** We compare TransIP and TransAug with different model sizes (Small/
301 Medium/Large) trained on the same number of samples from the OMol25 4M dataset and
302 report the evaluation metrics as a function of the processed number of atoms per second.
- 303 • **Extended training:** We train TransIP (Small) on the OMol25 4M dataset for 40 epochs
304 using 64 NVIDIA 80GB GPUs to evaluate its performance against standardized equivariant
305 baselines.

306 **Baselines.** We compare TransIP against: (i) an *unconstrained* TransIP variant trained with SO(3)
307 rotation augmentation to assess the impact of learned latent equivariance versus data augmentations,
308 and (ii) state-of-the-art equivariant models on OMol25: eSCN (Fu et al., 2025) in small/medium con-
309 figurations with both direct and energy-conserving force variants as well as GemNet-OC (Gasteiger
310 et al., 2022).

312 **Evaluation metrics.** Following the OMol25 official benchmark, we report: Force MAE (meV/Å),
313 Force cosine similarity, Energy per atom MAE (meV/atom), and Total energy MAE (meV). Detailed
314 metric definitions are provided in Appendix A.4.

316 6 RESULTS AND DISCUSSION
317318 6.1 SCALING DATA SIZE
319

320 To assess how performance scales with different training dataset sizes, we compare our latent
321 equivariance-based model (TransIP) against an unconstrained baseline that uses SO(3) data aug-
322 mentation (TransAug). Both models use a (small) 14M parameter Transformer architecture. Given
323 our tight compute budget, we train on 1M, 2M, and 4M OMol25 molecules for 5 epochs and report
324 validation (*Val-Comp*) results.

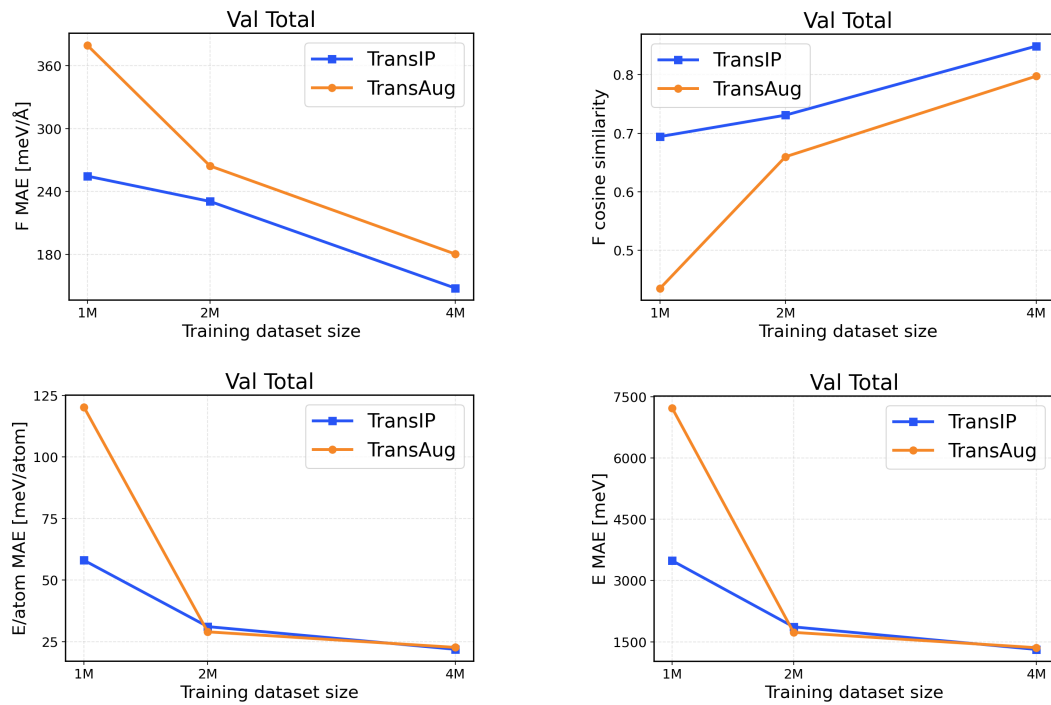


Figure 2: Val-Comp performance across different dataset sizes (1M / 2M / 4M): The top row presents force metrics, while the bottom row reports energy metrics.

Performance in a limited data regime. Figure 2 shows that TransIP delivers large gains when trained on 1M samples and outperforms TransAug across all evaluation metrics with a large margin on the total validation split. We also include the performance comparison for each molecule category in Appendix B. In Figure 2, the learned latent equivariance objective provides substantial improvements in force MAE (255 meV/Å vs 600 meV/Å MAE) and directional consistency (0.7 vs 0.44 force cosine similarity). Energy predictions also benefit from the latent equivariance objective, with TransIP achieving 58 meV/atom compared to TransAug’s 120 meV/atom. These results suggest that learning equivariance in a latent space is a more effective scheme to incorporate molecular symmetry than data augmentation, particularly when training data is limited.

Performance in a larger data regime. As we scale to 2M and 4M molecules, both models (TransIP and TransAug) improve across the evaluation metrics. However, on larger datasets, TransIP still achieves better force MAEs and cosine similarity metrics compared to TransAug. This might indicate that the learned transformation network can successfully capture the geometric relationships necessary for accurate force predictions. Notably, energy prediction performance converges between the two at larger data scales, with both methods achieving comparable per-atom MAE values. This convergence suggests that while learned equivariance provides crucial benefits for force-related metrics in all data regimes, its advantages for energy prediction become less pronounced as the model can learn invariant energy representations from sufficient augmented data.

6.2 LEARNED LATENT EQUIVARIANCE

We investigate how learned equivariance affects the embedding space in relation to validation performance as the data scale increases. Figure 3 plots each metric against latent equiv. error for TransIP (Small) trained for 5 epochs on 1M, 2M, and 4M molecules (see Table 3 for a detailed definition of each model configuration).

Lower latent equivariance error leads to better accuracy. We found that the learned equiv. error serves as a strong predictor of model performance. Across all metrics, we observe a clear monotonic trend: lower equiv. error is associated with better performance (Figure 3). However, energy and force predictions respond differently to improvements in equivariance. Energy predictions

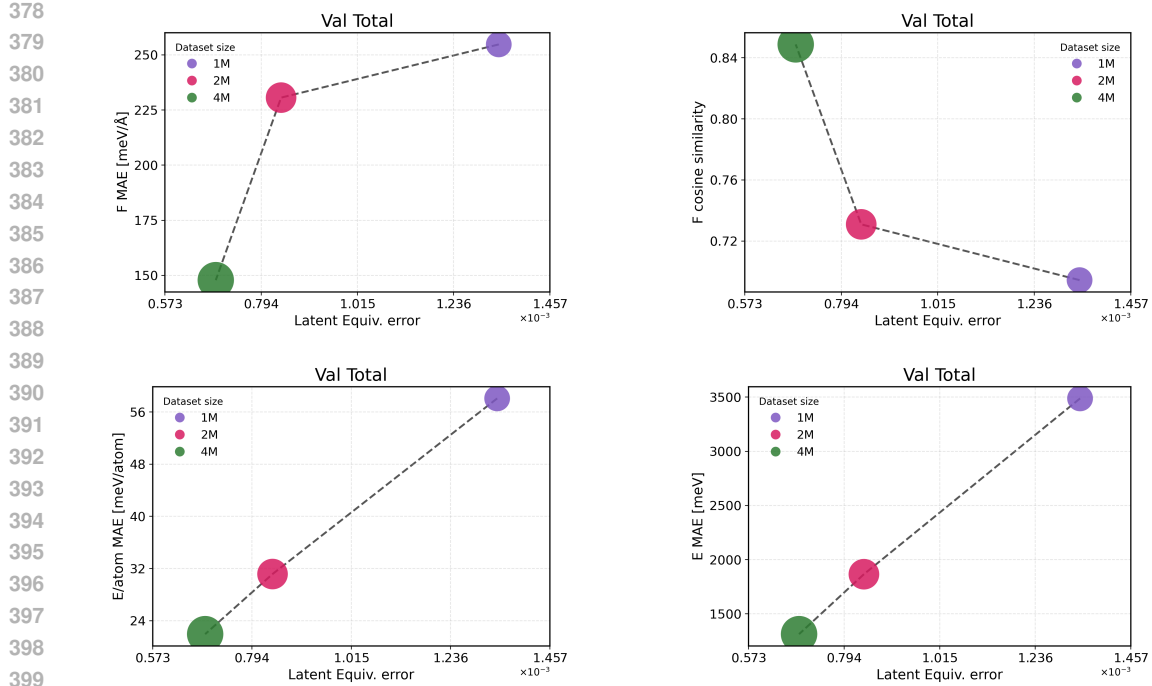


Figure 3: Latent equivariance (embedding) error versus validation performance. The top row reports force metrics, while the bottom row presents energy metrics.

show near-linear scaling with equiv. error, indicating that energy accuracy is directly limited by equivariance quality. This strong coupling aligns with energies being scalar invariants that depend primarily on learning correct symmetry-preserving features. In contrast, force predictions exhibit a two-regime behavior: initial improvements in equivariance (1M → 2M) yield modest force improvements, while further tightening of equivariance (2M → 4M) produces disproportionate gains. This might indicate that forces require both accurate equivariant features and sufficient data diversity to learn the energy landscape’s geometry.

These results demonstrate that implicitly learning equivariance through our learned transformation network provides an efficient inductive bias, accelerating learning. The 48% reduction in equiv. error from 1M to 4M training examples translates to 40-60% performance improvements, being more efficient than what would be expected from data scaling alone.

Learning equivariance leads to faster inference. To measure the inference efficiency of our method, we compare TransIP and TransAug with different model sizes (Small/Medium/Large) trained on 4M samples and report the evaluation metrics as a function of the processed number of atoms per second. However, due to limited compute, we compare models under a *fixed training budget* (i.e., with the same number of samples), which is 10k, 25k, and 100k steps for our Small, Medium, and Large models, respectively.

From the results in Figure 4, we see that TransIP scales smoothly with parameter count despite limited training: As model size grows, performance improves across all metrics. In contrast, TransAug exhibits poorer scaling—larger models perform worse than smaller ones, with the Large model configuration yielding the lowest performance. This might indicate that augmentation alone does not provide a sufficiently informative and stable inductive bias for large-capacity models trained for molecular force field prediction.

6.3 ARCHITECTURAL EQUIVARIANCE VERSUS LEARNED EQUIVARIANCE

Table 1 compares the energy and force prediction performance of **TransIP-S (Small)** against **TransAug-S (Small)** as well as several well-known equivariant baselines for the OMol 2M Val-Comp evaluation dataset. The results of this comparison demonstrate that **TransIP-S** outperforms

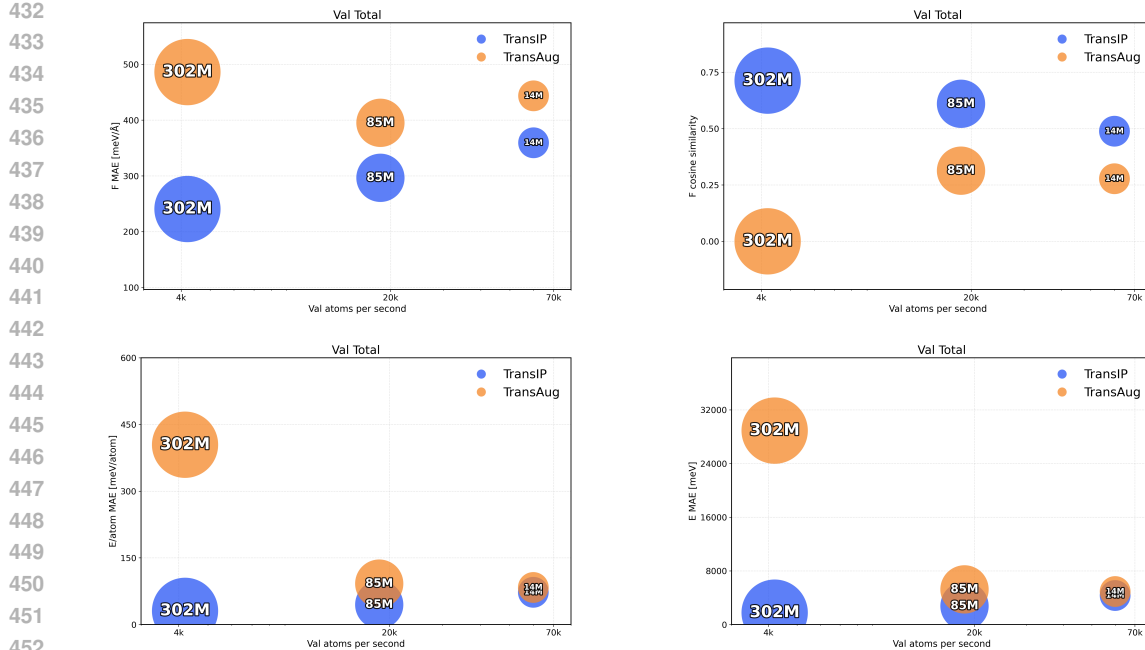


Figure 4: Validation total inference trade-off (atoms/s versus performance). The top row presents force metrics, while the bottom row represents energy metrics.

| Model | Epochs | Biomolecules | | Electrolytes | | Metal Complexes | | Neutral Organics | | Total | |
|---------------|--------|--------------|----------|--------------|----------|-----------------|----------|------------------|----------|----------|----------|
| | | Energy ↓ | Forces ↓ | Energy ↓ | Forces ↓ | Energy ↓ | Forces ↓ | Energy ↓ | Forces ↓ | Energy ↓ | Forces ↓ |
| eSEN-sm-d. | 80 | 0.88 | 8.12 | 1.93 | 12.64 | 3.37 | 40.44 | 2.16 | 20.17 | 2.19 | 13.01 |
| eSEN-sm-cons. | 80 | 0.86 | 6.17 | 1.61 | 11.16 | 2.72 | 35.33 | 1.50 | 16.92 | 1.89 | 11.10 |
| eSEN-md-d. | 80 | 0.47 | 3.38 | 1.18 | 6.51 | 2.53 | 27.31 | 1.21 | 9.26 | 1.32 | 6.78 |
| GemNet-OC-r6 | 80 | 0.40 | 5.84 | 1.39 | 9.37 | 2.74 | 33.60 | 1.88 | 16.55 | 1.41 | 9.83 |
| GemNet-OC | 80 | 0.25 | 5.20 | 1.04 | 8.42 | 2.66 | 32.76 | 1.64 | 15.59 | 1.13 | 8.98 |
| TransAug-S | 5 | 16.6 | 219.3 | 17.5 | 161.9 | 20.7 | 150.6 | 28.9 | 218.8 | 23.5 | 180.3 |
| TransIP-S | 5 | 17.3 | 181.1 | 15.9 | 129.6 | 18.5 | 132.5 | 23.5 | 165.0 | 22.3 | 146.6 |
| TransIP-S | 40 | 13.8 | 121.5 | 12.7 | 94.0 | 15.2 | 105.6 | 18.5 | 125.4 | 17.9 | 103.8 |
| TransIP-S | 80 | 10.5 | 103.2 | 10.2 | 82.4 | 13.8 | 96.1 | 16.0 | 111.4 | 14.2 | 90.1 |
| TransIP-M | 60 | 6.3 | 35.2 | 5.7 | 33.0 | 7.4 | 58.5 | 7.9 | 51.0 | 8.1 | 35.4 |

Table 1: Comprehensive Val-Comp energy and force MAE results.

TransAug-S (trained for 5 epochs) in all but one evaluation metric, particularly differentiating itself in terms of force prediction (we include the performance comparison for SPICE and reactivity splits in Table 7). We further report the performance of TransIP-S trained for 40 epochs and 80 epochs as well as TransIP-M for 60 epochs (for fair comparison to each equivariant baseline). Results with TransIP-M after 60 training epochs suggest steady improvement is likely to be observed during the remainder of the model’s training epochs, which, despite limited compute, we are currently working towards. We also report the inference speed for our TransIP versions and eSEN baseline using the same hardware with 8 A100 GPUs in Table 2. For eSEN, we follow the small version indicated by Levine et al. (2025) with hyperparameters in Table 4. Both TransIP’s small and medium versions are significantly faster than the eSEN baseline, while TransIP-L is slightly faster than eSEN.

| | TransIP-S | TransIP-M | TransIP-L | eSEN |
|-------------------|-----------|-----------|-----------|-------|
| Approx. atoms/sec | 60,000 | 18,500 | 4,200 | 3,900 |

Table 2: Inference speed for TransIP variants and eSEN baseline.

486 7 WHAT TRANSIP LEARNS

488 To understand the structure of learned equivariance, we ask whether the effect of rotating different
 489 inputs can be explained by a *single* group action in the latent space; i.e., whether there exists a rep-
 490 resentation $\rho(g) : \mathbb{R}^d \rightarrow \mathbb{R}^d$ such that $f(\phi(g)(m)) \approx \rho(g) f(m)$, where $f_\theta : \mathcal{M} \rightarrow \mathbb{R}^d$ denotes
 491 the embedding network, and $g \in \text{SO}(3)$ acts on a molecule m via the input representation $\phi(g)$ (ro-
 492 tation of atomic coordinates). Because $\rho(g)$ is unknown, we compute an approximate group action
 493 $\widehat{\rho}(g) \in \text{O}(d)$ by solving an orthogonal Procrustes problem on embeddings from 100 validation sam-
 494 ples (obtained from a trained TransIP model). Writing $Z = [f(m_1)^\top, \dots, f(m_n)^\top]$, $Z_g =$
 495 $[f(\phi(g)(m_1))^\top, \dots, f(\phi(g)(m_n))^\top]$, we first pool-whiten the two views (shared mean and stan-
 496 dard deviation per channel) and then solve $\widehat{\rho}(g) = \arg \min_{Q \in \text{O}(d)} \|\widetilde{Z}Q - \widetilde{Z}_g\|_F^2$, which has the
 497 closed form $\widehat{\rho}(g) = UV^\top$ for the SVD of $\widetilde{Z}^\top \widetilde{Z}_g = U\Sigma V^\top$.

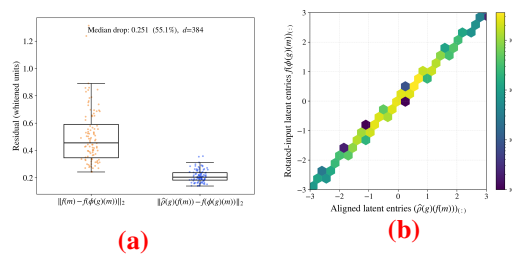
498 In Figure 5a, we report per-molecule residuals
 499 before alignment, $\|f(m) - f(\phi(g)(m))\|_2$,
 500 and after applying the global orthogonal map,
 501 $\|\widehat{\rho}(g)f(m) - f(\phi(g)(m))\|_2$. A left→right
 502 drop in the distribution indicates that a single
 503 orthogonal transform explains most of the
 504 rotation-induced change in the embedding. In
 505 Figure 5b, we compare the channel-level rela-
 506 tion by plotting a hexbin density of all pairs
 507 $(\widehat{\rho}(g)f(m))_k, (f(\phi(g)(m)))_k, k =$
 508 $1, \dots, d$, $m \in \text{val}$. where color encodes the
 509 log count of points in each hexagonal bin. A
 510 tight diagonal concentration after the single
 511 global alignment $\widehat{\rho}(g)$ might suggest that the
 512 two views are almost identical at entrywise-
 513 level and the group action in latent space is *ap-
 514 proximately orthogonal* and shared across dif-
 515 ferent molecules.

516 **Takeaways.** Figure 5a shows that the magnitude of the rotation-induced discrepancy of different
 517 molecules drops after a single orthogonal alignment, and Figure 5b shows that the aligned channels
 518 match entrywise, concentrating along the identity. These results indicate that TransIP learns an
 519 embedding where input rotations act approximately as a shared orthogonal transformation, even
 520 though explicit equivariance was not enforced in the architecture.

521 8 CONCLUSION

522 In this work, we introduced TransIP for modeling interatomic potentials with a modern Transformer-
 523 based architecture and a scalable latent equivariance objective. Empirical results across a variety of
 524 chemical systems as well as model and dataset scales suggest that TransIP’s latent equivariance
 525 objective enables better performance scaling than popular data augmentation-based alternatives to
 526 learning geometric equivariance. Further, we find that improvements in learning latent equivariance
 527 are strongly related to improved modeling of interatomic potentials, suggesting a complementary
 528 nature between the two prediction objectives. With sufficient compute, future work could involve
 529 studying the performance of TransIP in larger data, modeling, and runtime regimes in addition to the
 530 behavior of TransIP in a context amenable to the double-descent phenomenon (Power et al., 2022).

531 While equivariant models for molecular machine learning have recently gained much research in-
 532 terest, with the large amount of data being generated and the need for larger model sizes, it is also
 533 important that models used for interatomic potentials be highly scalable. Through our work, we have
 534 shown that the generic Transformer is capable of modeling molecules accurately but is also able to
 535 learn equivariance effectively through our novel latent objective, all while being highly scalable. By
 536 making our code openly available to the research community, we hope that our work inspires future
 537 research that explores ways to leverage the simpler and more scalable Transformer architecture to
 538 better model equivariant molecular properties through learned equivariance.



539 **Figure 5: Group action in the embedding**
 540 **space.** (a) Per-molecule residuals before align-
 541 ment, $\|f(m) - f(\phi(g)(m))\|_2$, and after apply-
 542 ing a global orthogonal map $\widehat{\rho}(g)$ on pool-whitened
 543 latents, $\|\widehat{\rho}(g)f(m) - f(\phi(g)(m))\|_2$. (b) Entry-
 544 wise comparison: hexbin density of $(\widehat{\rho}(g)f(m))_{(:,)}$
 545 vs. $f(\phi(g)(m))_{(:,)}$, pooled over molecules’ embed-
 546 dings.

540 9 ETHICS STATEMENT 541

542 This work focuses on developing scalable machine-learned interatomic potentials (MLIPs). Our
543 contributions are based on the principle of equivariance and do not involve sensitive personal data,
544 human subjects, or personally identifiable information. The dataset used, OMol25, is an open-source
545 quantum chemistry benchmark for research use. The potential broader impacts of our method are
546 that it can accelerate research in drug discovery and material sciences. By making MLIP models
547 cheaper to train, we make molecular modeling more accessible to the broader research community.
548 However, misuse in safety-critical applications like drug discovery could lead to adverse outcomes.
549 No dual-use is identified beyond the general risks of over-reliance on approximate ML models in
550 scientific workflows.

551 10 REPRODUCIBILITY STATEMENT 552

553 **Dataset:** All experiments were conducted on the Open Molecules 2025 (OMol25) dataset, which is
554 publicly available and documented ([Levine et al., 2025](#)). We follow its official training and validation
555 splits (4M train dataset, 2M out-of-distribution validation dataset).

556 **Architectures and hyperparameters:** We include detailed architectural configurations (e.g., model
557 sizes, layers, hidden dimensions, attention heads) in Appendix [A](#).

558 **Evaluation:** We report standardized OMol25 metrics: Force MAE, Force cosine similarity, Energy
559 per atom MAE, and Total Energy MAE.

560 **Code and models:** We build our implementation on the FAIRCHEM framework for standardized
561 MLIP training and evaluation. However, we also plan to release our code as an open-source reposi-
562 tory upon acceptance.

563 **Scaling experiments:** We perform scaling experiments with varying model and dataset sizes, with
564 corresponding results presented in Figures [2](#), [3](#), and [4](#).

565 **Compute resources:** Experiments were run on a limited number of NVIDIA A100 80GB GPUs.
566 Small-scale experiments used 8 GPUs for 5 epochs, while extended runs used 64 GPUs for up to 80
567 epochs (currently in progress).

571
572
573
574
575
576
577
578
579
580
581
582
583
584
585
586
587
588
589
590
591
592
593

594 REFERENCES
595

596 Jacob Abramson, Jane Adler, John Dunger, et al. Accurate structure prediction of biomolecular
597 interactions with alphafold 3. *Nature*, 630:493–500, 2024. doi: 10.1038/s41586-024-07487-w.
598 URL <https://doi.org/10.1038/s41586-024-07487-w>.

599 Brandon Anderson, Truong Son Hy, and Risi Kondor. Cormorant: Covariant molecular neu-
600 ral networks. In *Advances in Neural Information Processing Systems*, volume 32. Curran
601 Associates, Inc., 2019. URL https://proceedings.neurips.cc/paper_files/paper/2019/file/03573b32b2746e6e8ca98b9123f2249b-Paper.pdf.

602 603

604 Justin Baker, Shih-Hsin Wang, Tommaso de Fernex, and Bao Wang. An explicit frame construction
605 for normalizing 3d point clouds. In *Forty-first International Conference on Machine Learning*,
606 2024. URL <https://openreview.net/forum?id=SZ0JnRxi0x>.

607 608

609 Ilyes Batatia, David Peter Kovacs, Gregor N. C. Simm, Christoph Ortner, and Gabor Csanyi. MACE:
610 Higher order equivariant message passing neural networks for fast and accurate force fields. In
611 Alice H. Oh, Alekh Agarwal, Danielle Belgrave, and Kyunghyun Cho (eds.), *Advances in Neu-
612 ral Information Processing Systems*, 2022. URL <https://openreview.net/forum?id=YPpSngE-ZU>.

613 614

615 Simon Batzner, Albert Musaelian, Lixin Sun, et al. E(3)-equivariant graph neural net-
616 works for data-efficient and accurate interatomic potentials. *Nature Communications*, 13:
617 2453, 2022. doi: 10.1038/s41467-022-29939-5. URL <https://doi.org/10.1038/s41467-022-29939-5>.

618 619

620 Johannes Brandstetter, Rob Hesselink, Elise van der Pol, Erik J Bekkers, and Max Welling. Geomet-
621 ric and physical quantities improve e(3) equivariant message passing. In *International Confer-
622 ence on Learning Representations*, 2022. URL https://openreview.net/forum?id=_xwr8gOBeV1.

623 624

625 Jiacheng Cen, Anyi Li, Ning Lin, Yuxiang Ren, Zihe Wang, and Wenbing Huang. Are high-
626 degree representations really unnecessary in equivariant graph neural networks? In *The Thirty-
627 eighth Annual Conference on Neural Information Processing Systems*, 2024. URL <https://openreview.net/forum?id=M0ncNVuGYN>.

628 629

630 Lowik Chanussot, Abhishek Das, Siddharth Goyal, Thibaut Lavril, Muhammed Shuaibi, Morgane
631 Riviere, Kevin Tran, Javier Heras-Domingo, Caleb Ho, Weihua Hu, Aini Palizhati, Anuroop Sri-
632 ram, Brandon Wood, Junwoong Yoon, Devi Parikh, C. Lawrence Zitnick, and Zachary Ulissi.
633 Open catalyst 2020 (oc20) dataset and community challenges. *ACS Catalysis*, 11(10):6059–6072,
634 May 2021. ISSN 2155-5435. doi: 10.1021/acscatal.0c04525. URL <http://dx.doi.org/10.1021/acscatal.0c04525>.

635 636

637 Stefan Chmiela, Valentin Vassilev-Galindo, Oliver T. Unke, Adil Kabylda, Huziel E. Sauceda,
638 Alexandre Tkatchenko, and Klaus-Robert Müller. Accurate global machine learning force fields
639 for molecules with hundreds of atoms, 2022. URL <https://arxiv.org/abs/2209.14865>.

640 641

642 Anders S. Christensen, Sai Krishna Sirumalla, Zhuoran Qiao, Michael B. O’Connor, Daniel G. A.
643 Smith, Feizhi Ding, Peter J. Bygrave, Animashree Anandkumar, Matthew Welborn, Frederick R.
644 Manby, and Thomas F. Miller. Orbnet denali: A machine learning potential for biological and
645 organic chemistry with semi-empirical cost and dft accuracy. *The Journal of Chemical Physics*,
646 155(20), November 2021. ISSN 1089-7690. doi: 10.1063/5.0061990. URL <http://dx.doi.org/10.1063/5.0061990>.

647 648

649 Taco S. Cohen and Max Welling. Steerable CNNs. In *International Conference on Learning Rep-
650 resentations*, 2017. URL <https://openreview.net/forum?id=rJQKYt5ll>.

651 652

653 Volker L. Deringer, Miguel A. Caro, and Gábor Csányi. Machine learning interatomic potentials as
654 emerging tools for materials science. *Advanced Materials*, 2019.

648 Christian Devereux, Justin Smith, Kate Davis, Kipton Barros, Roman Zubatyuk, Olexandr Isayev,
 649 and Adrian Roitberg. Extending the applicability of the ani deep learning molecular potential
 650 to sulfur and halogens. *Journal of Chemical Theory and Computation*, XXXX, 06 2020. doi:
 651 10.1021/acs.jctc.0c00121.

652 Alexey Dosovitskiy, Lucas Beyer, Alexander Kolesnikov, Dirk Weissenborn, Xiaohua Zhai, Thomas
 653 Unterthiner, Mostafa Dehghani, Matthias Minderer, Georg Heigold, Sylvain Gelly, Jakob Uszkoreit,
 654 and Neil Houlsby. An image is worth 16x16 words: Transformers for image recogni-
 655 tion at scale. In *International Conference on Learning Representations*, 2021. URL <https://openreview.net/forum?id=YicbFdNTTy>.

656

657 Alexandre Agm Duval, Victor Schmidt, Alex Hernández-García, Santiago Miret, Fragkiskos D.
 658 Malliaros, Yoshua Bengio, and David Rolnick. FAENet: Frame averaging equivariant GNN for
 659 materials modeling. In *Proceedings of the 40th International Conference on Machine Learning*,
 660 2023. URL <https://proceedings.mlr.press/v202/duval23a.html>.

661

662 Nadav Dym, Hannah Lawrence, and Jonathan W. Siegel. Equivariant frames and the impossibility
 663 of continuous canonicalization. In *ICML*, 2024. URL <https://openreview.net/forum?id=4iy0q0carb>.

664

665 Peter Eastman, Pavan Kumar Behara, David L. Dotson, Raimondas Galvelis, John E. Herr, Josh T.
 666 Horton, Yuezhi Mao, John D. Chodera, Benjamin P. Pritchard, Yuanqing Wang, Gianni De Fab-
 667 ritiis, and Thomas E. Markland. Spice, a dataset of drug-like molecules and peptides for training
 668 machine learning potentials, 2022. URL <https://arxiv.org/abs/2209.10702>.

669

670 Peter Eastman, Benjamin P. Pritchard, John D. Chodera, and Thomas E. Markland. Nutmeg and
 671 spice: Models and data for biomolecular machine learning, 2024. URL <https://arxiv.org/abs/2406.13112>.

672

673 Xiang Fu, Brandon M Wood, Luis Barroso-Luque, Daniel S. Levine, Meng Gao, Misko Dzamba,
 674 and C. Lawrence Zitnick. Learning smooth and expressive interatomic potentials for physical
 675 property prediction. In *Forty-second International Conference on Machine Learning*, 2025. URL
 676 <https://openreview.net/forum?id=R0PBjxIbgm>.

677

678 Fabian B. Fuchs, Daniel E. Worrall, Volker Fischer, and Max Welling. Se(3)-transformers: 3d roto-
 679 translation equivariant attention networks. In *Advances in Neural Information Processing Systems*
 680 34 (NeurIPS), 2020.

681

682 Johannes Gasteiger, Janek Groß, and Stephan Günnemann. Directional message passing for molec-
 683 ular graphs. In *International Conference on Learning Representations*, 2020. URL <https://openreview.net/forum?id=BleWbxStPH>.

684

685 Johannes Gasteiger, Muhammed Shuaibi, Anuroop Sriram, Stephan Günnemann, Zachary Ward
 686 Ulissi, C. Lawrence Zitnick, and Abhishek Das. Gemnet-OC: Developing graph neural networks
 687 for large and diverse molecular simulation datasets. *Transactions on Machine Learning Research*,
 688 2022. ISSN 2835-8856. URL <https://openreview.net/forum?id=u8tvSxm4Bs>.

689

690 Tinglin Huang, Zhenqiao Song, Rex Ying, and Wengong Jin. Protein-nucleic acid complex modeling
 691 with frame averaging transformer. In *The Thirty-eighth Annual Conference on Neural Information
 692 Processing Systems*, 2024. URL <https://openreview.net/forum?id=Xngi3Z3wkN>.

693

694 Hiroshi Inoue. Data augmentation by pairing samples for images classification, 2018. URL <https://arxiv.org/abs/1801.02929>.

695

696 Ryan Jacobs, Dane Morgan, Siamak Attarian, Jun Meng, Chen Shen, Zhenghao Wu, Clare Yijia
 697 Xie, Julia H. Yang, Nongnuch Artrith, Ben Blaiszik, Gerbrand Ceder, Kamal Choudhary, Gabor
 698 Csanyi, Ekin Dogus Cubuk, Bowen Deng, Ralf Drautz, Xiang Fu, Jonathan Godwin, Vasant
 699 Honavar, Olexandr Isayev, Anders Johansson, Boris Kozinsky, Stefano Martiniani, Shyue Ping
 700 Ong, Igor Poltavsky, KJ Schmidt, So Takamoto, Aidan P. Thompson, Julia Westermayr, and
 701 Brandon M. Wood. A practical guide to machine learning interatomic potentials – status and
 702 future. *Current Opinion in Solid State and Materials Science*, 35:101214, March 2025. ISSN
 703 1359-0286. doi: 10.1016/j.cossms.2025.101214. URL <http://dx.doi.org/10.1016/j.cossms.2025.101214>.

702 Chaitanya K. Joshi, Cristian Bodnar, Simon V Mathis, Taco Cohen, and Pietro Lio. On the expressive
 703 power of geometric graph neural networks. In *Proceedings of the 40th International Conference on Machine Learning*, 2023. URL <https://proceedings.mlr.press/v202/joshi23a.html>.

704

705

706 Chaitanya K. Joshi, Xiang Fu, Yi-Lun Liao, Vahe Gharakhanyan, Benjamin Kurt Miller, Anuroop
 707 Sriram, and Zachary W. Ulissi. All-atom diffusion transformers: Unified generative modelling of
 708 molecules and materials. In *International Conference on Machine Learning*, 2025.

709

710 Sékou-Oumar Kaba, Arnab Kumar Mondal, Yan Zhang, Yoshua Bengio, and Siamak Ravanbakhsh.
 711 Equivariance with learned canonicalization functions. In *NeurIPS 2022 Workshop on Symmetry
 712 and Geometry in Neural Representations*, 2022. URL <https://openreview.net/forum?id=pVD1k8ge25a>.

713

714

715 Johannes Klicpera, Florian Becker, and Stephan Günnemann. Gemnet: Universal directional
 716 graph neural networks for molecules. In A. Beygelzimer, Y. Dauphin, P. Liang, and J. Wort-
 717 man Vaughan (eds.), *Advances in Neural Information Processing Systems*, 2021. URL https://openreview.net/forum?id=HS_sOaxS9K-.

718

719 Niklas Leimeroth, Linus C. Erhard, Karsten Albe, and Jochen Rohrer. Machine-learning interatomic
 720 potentials from a users perspective: A comparison of accuracy, speed and data efficiency, 2025.
 721 URL <https://arxiv.org/abs/2505.02503>.

722

723 Daniel S. Levine, Muhammed Shuaibi, Evan Walter Clark Spotte-Smith, Michael G. Taylor,
 724 Muhammad R. Hasyim, Kyle Michel, Ilyes Batatia, Gábor Csányi, Misko Dzamba, Peter East-
 725 man, Nathan C. Frey, Xiang Fu, Vahe Gharakhanyan, Aditi S. Krishnapriyan, Joshua A. Rackers,
 726 Sanjeev Raja, Ammar Rizvi, Andrew S. Rosen, Zachary Ulissi, Santiago Vargas, C. Lawrence
 727 Zitnick, Samuel M. Blau, and Brandon M. Wood. The open molecules 2025 (omol25) dataset,
 728 evaluations, and models, 2025. URL <https://arxiv.org/abs/2505.08762>.

729

730 Yi-Lun Liao and Tess Smidt. Equiformer: Equivariant graph attention transformer for 3d atom-
 731 istic graphs. In *International Conference on Learning Representations*, 2023. URL <https://openreview.net/forum?id=KwmPfARgOTD>.

732

733 Yi-Lun Liao, Brandon Wood, Abhishek Das*, and Tess Smidt*. EquiformerV2: Improved Equiv-
 734 ariant Transformer for Scaling to Higher-Degree Representations. In *International Conference on
 735 Learning Representations (ICLR)*, 2024a. URL <https://openreview.net/forum?id=mCOBKZmrzD>.

736

737 Yi-Lun Liao et al. EquiformerV2: Improved equivariant transformer for scaling 3d molecular learn-
 738 ing. *arXiv preprint arXiv:2402.xxxxx*, 2024b.

739

740 Yuchao Lin, Jacob Helwig, Shurui Gui, and Shuiwang Ji. Equivariance via minimal frame averaging
 741 for more symmetries and efficiency. In *Forty-first International Conference on Machine Learning*,
 742 2024. URL <https://openreview.net/forum?id=guFsTBXsov>.

743

744 Peter Lippmann, Gerrit Gerhartz, Roman Remme, and Fred A Hamprecht. Beyond
 745 canonicalization: How tensorial messages improve equivariant message pass-
 746 ing. In *International Conference on Representation Learning*, volume 2025, 2025.
 747 URL https://proceedings.iclr.cc/paper_files/paper/2025/file/db7534a06ace69f4ec95bc89e91d5dbb-Paper-Conference.pdf.

748

749 George Ma, Yifei Wang, Derek Lim, Stefanie Jegelka, and Yisen Wang. A canonicalization per-
 750 spective on invariant and equivariant learning. In *The Thirty-eighth Annual Conference on Neu-
 751 ral Information Processing Systems*, 2024. URL <https://openreview.net/forum?id=jjcY92FX4R>.

752

753 Moin Uddin Maruf, Sungmin Kim, and Zeeshan Ahmad. Learning long-range interactions in equiv-
 754 ariant machine learning interatomic potentials via electronic degrees of freedom. *The Journal of
 755 Physical Chemistry Letters*, 16(35):9078–9087, August 2025. ISSN 1948-7185. doi: 10.1021/acs.jpclett.5c02352. URL <http://dx.doi.org/10.1021/acs.jpclett.5c02352>.

756 Arslan Mazitov, Filippo Bigi, Matthias Kellner, Paolo Pegolo, Davide Tisi, Guillaume Fraux, Sergey
 757 Pozdnyakov, Philip Loche, and Michele Ceriotti. Pet-mad, a lightweight universal interatomic
 758 potential for advanced materials modeling, 2025. URL <https://arxiv.org/abs/2503.14118>.

759

760 Albert Musaelian, Sebastian Batzner, Anders Johansson, Simon Kozinsky, and Boris Kozinsky.
 761 Learning local 3d energetics with graph neural networks. *Nature Communications*, 2023.

762

763 Misgana Negassi, Diane Wagner, and Alexander Reiterer. Smart(sampling)augment: Optimal and
 764 efficient data augmentation for semantic segmentation. *Algorithms*, 15(5), 2022. ISSN 1999-
 765 4893. doi: 10.3390/a15050165. URL <https://www.mdpi.com/1999-4893/15/5/165>.

766

767 Frank Noé, Alexandre Tkatchenko, Klaus-Robert Müller, and Cecilia Clementi. Machine learning
 768 for molecular simulation. *Annual Review of Physical Chemistry*, 71(1):361–390, April 2020.
 769 ISSN 1545-1593. doi: 10.1146/annurev-physchem-042018-052331. URL <http://dx.doi.org/10.1146/annurev-physchem-042018-052331>.

770

771 Saro Passaro and C. Lawrence Zitnick. Reducing $so(3)$ convolutions to $so(2)$ for efficient equivariant
 772 gnns. In *Proceedings of the 40th International Conference on Machine Learning*, ICML’23.
 773 JMLR.org, 2023a.

774

775 Saro Passaro and C. Lawrence Zitnick. Reducing $SO(3)$ convolutions to $SO(2)$ for efficient equivariant
 776 GNNs. In *Proceedings of the 40th International Conference on Machine Learning*, Proceedings of Machine Learning Research. PMLR, 2023b.

777

778 Alethea Power, Yuri Burda, Harri Edwards, Igor Babuschkin, and Vedant Misra. Grokking: Gen-
 779 eralization beyond overfitting on small algorithmic datasets. *arXiv preprint arXiv:2201.02177*,
 780 2022.

781

782 Omri Puny, Matan Atzmon, Edward J. Smith, Ishan Misra, Aditya Grover, Heli Ben-Hamu, and
 783 Yaron Lipman. Frame averaging for invariant and equivariant network design. In *International
 784 Conference on Learning Representations*, 2022. URL <https://openreview.net/forum?id=zIUyj55nXR>.

785

786

787 Eric Qu and Aditi Krishnapriyan. The importance of being scalable: Improving the speed and
 788 accuracy of neural network interatomic potentials across chemical domains. *Advances in Neural
 789 Information Processing Systems*, 37:139030–139053, 2024.

790

791 Fazle Rahat, M Shifat Hossain, Md Rubel Ahmed, Sumit Kumar Jha, and Rickard Ewetz. Data
 792 augmentation for image classification using generative ai, 2024. URL <https://arxiv.org/abs/2409.00547>.

793

794 Benjamin Rhodes, Sander Vandenhante, Vaidotas Šimkus, James Gin, Jonathan Godwin, Tim
 795 Duignan, and Mark Neumann. Orb-v3: atomistic simulation at scale, 2025. URL <https://arxiv.org/abs/2504.06231>.

796

797

798 Alvaro Sanchez-Gonzalez, Jonathan Godwin, Tobias Pfaff, Rex Ying, Jure Leskovec, and Peter W.
 799 Battaglia. Learning to simulate complex physics with graph networks. In *Proceedings of the 37th
 800 International Conference on Machine Learning*. JMLR.org, 2020.

801

802 Victor Garcia Satorras, Emiel Hoogeboom, and Max Welling. $E(n)$ equivariant graph neural net-
 803 works. In *Proceedings of the 38rd International Conference on Machine Learning*, 2021.

804

805 Mathias Schreiner, Arghya Bhownik, Tejs Vegge, Jonas Busk, and Ole Winther. Transition1x –
 806 a dataset for building generalizable reactive machine learning potentials, 2022. URL <https://arxiv.org/abs/2207.12858>.

807

808 Kristof T. Schütt, Huziel E. Sauceda, P.-J. Kindermans, Alexandre Tkatchenko, and Klaus-Robert
 809 Müller. Schnet: A continuous-filter convolutional neural network for modeling quantum interac-
 810 tions. In *NeurIPS*, 2017.

810 Muhammed Shuaibi, Abhishek Das, Anuroop Sriram, Misko, Luis Barroso-Luque, Ray Gao, Sid-
 811 dharth Goyal, Zachary Ulissi, Brandon Wood, Tian Xie, Junwoong Yoon, Brook Wander, Adeesh
 812 Kolluru, Richard Barnes, Ethan Sunshine, Kevin Tran, Xiang, Daniel Levine, Nima Shoghi, Ilias
 813 Chair, , Janice Lan, Kaylee Tian, Joseph Musielewicz, clz55, Weihua Hu, , Kyle Michel, willis,
 814 and vbtchr. FAIRChem, 2025. URL <https://github.com/facebookresearch/fairchem>.

815

816 Jianlin Su, Yu Lu, Shengfeng Pan, Ahmed Murtadha, Bo Wen, and Yunfeng Liu. Roformer: En-
 817 hanced transformer with rotary position embedding, 2023. URL <https://arxiv.org/abs/2104.09864>.

818

819 Philipp Thölke and Gianni De Fabritiis. Equivariant transformers for neural network based molec-
 820 ular potentials. In *International Conference on Learning Representations*, 2022. URL <https://openreview.net/forum?id=zNHzqZ9wrRB>.

821

822 Nathaniel Thomas, Tess Smidt, Steven Kearnes, Lusann Yang, Li Li, Kai Kohlhoff, and Patrick
 823 Riley. Tensor field networks: Rotation- and translation-equivariant neural networks for 3d point
 824 clouds, 2018. URL <https://arxiv.org/abs/1802.08219>.

825

826 Oliver T. Unke and Markus Meuwly. Physnet: A neural network for predicting energies, forces,
 827 dipole moments, and partial charges. *Journal of Chemical Theory and Computation*, 15(6):
 828 3678–3693, May 2019. ISSN 1549-9626. doi: 10.1021/acs.jctc.9b00181. URL <http://dx.doi.org/10.1021/acs.jctc.9b00181>.

829

830

831 Yuyang Wang, Ahmed A. Elhag, Navdeep Jaitly, Joshua M. Susskind, and Miguel Ángel Bautista.
 832 Swallowing the bitter pill: Simplified scalable conformer generation. In *Forty-first International
 833 Conference on Machine Learning*, 2024.

834

835 Ziduo Yang, Xian Wang, Yifan Li, Qiuje Lv, Calvin Yu-Chian Chen, and Lei Shen. Efficient
 836 equivariant model for machine learning interatomic potentials. *npj Computational Materials*,
 837 11(1):49, 2025. doi: 10.1038/s41524-025-01535-3. URL <https://doi.org/10.1038/s41524-025-01535-3>.

838

839 Xinyi Yu, Guanbin Li, Wei Lou, Siqi Liu, Xiang Wan, Yan Chen, and Haofeng Li. Diffusion-based
 840 data augmentation for nuclei image segmentation. In *Medical Image Computing and Computer
 841 Assisted Intervention – MICCAI 2023*, 2023.

842

843 Leo Zhang, Kianoosh Ashouritaklimi, Yee Whye Teh, and Rob Cornish. Symdiff: Equivariant
 844 diffusion via stochastic symmetrisation. In *The Thirteenth International Conference on Learning
 845 Representations*, 2025a. URL <https://openreview.net/forum?id=i1NNCrRxdM>.

846

847 Linfeng Zhang, Jiequn Han, Han Wang, Roberto Car, and Weinan E. Deep potential molecular
 848 dynamics: A scalable model with the accuracy of quantum mechanics. *Physical Review Letters*,
 849 120(14), April 2018. ISSN 1079-7114. doi: 10.1103/physrevlett.120.143001. URL <http://dx.doi.org/10.1103/PhysRevLett.120.143001>.

850

851 Shuhao Zhang, Roman Zubatyuk, Yinuo Yang, Adrian Roitberg, and Olexandr Isayev. Ani-1xbb:
 852 An ani-based reactive potential for small organic molecules. *Journal of chemical theory and
 853 computation*, 21, 04 2025b. doi: 10.1021/acs.jctc.5c00347.

854

855

856

857

858

859

860

861

862

863

864 **A IMPLEMENTATION DETAILS**865 **A.1 MODEL ARCHITECTURE**

866 Table 3 provides the complete architectural specifications for TransIP’s model versions, as well as
 867 **eSEN hyperparameters for the inference test in Table 2.** For eSEN, we follow the small version
 870 reported by Levine et al. (2025).

871 Table 3: TransIP model configurations. All versions share the same embedding method and activation
 872 functions.
 873

| 875 Configuration | 876 Small (S) | 877 Medium (M) | 878 Large (L) |
|--|---------------|----------------|---------------|
| 876 Hidden dimension (d) | 384 | 768 | 1024 |
| 877 Number of layers (L) | 8 | 12 | 24 |
| 878 Number of heads | 6 | 12 | 16 |
| 879 Total parameters | 14M | 85M | 302M |
| <i>880 Shared configurations:</i> | | | |
| 881 Coordinate embedding | | MLP | |
| 882 Activation function | | GELU | |
| 883 Context length | | 1024 | |
| 884 Projection dropout | | 0.01 | |
| 885 Attention dropout | | 0.0 | |
| <i>886 Transformation network \mathcal{T}_τ:</i> | | | |
| 887 Number of layers | | 2 | |
| 888 Hidden dimension | | $2 \times d$ | |
| 889 Activation | | GELU | |

890
891 Table 4: **eSEN hyperparameters for inference test in Table 2.**
892

| 893 Configuration | 894 Value |
|------------------------|-------------|
| 895 sphere_channels | 128 |
| 896 lmax | 2 |
| 897 mmax | 2 |
| 898 edge_channels | 128 |
| 899 distance_function | gaussian |
| 900 num_distance_basis | 64 |
| 901 num_layers | 4 |
| 902 hidden_channels | 128 |
| 903 max_neighbors | 30 |
| 904 cutoff_radius | 6 |
| 905 normalization_type | rms_norm_sh |
| 906 activation_type | gate |
| 907 ff_type | spectral |

908 **A.2 TRAINING HYPERPARAMETERS**

909 Table 5 provides TransIP’s optimal hyperparameters.
 910

911 **A.3 DATA PROCESSING AND AUGMENTATION**
912

913 TransIP processes molecular data with the following pipeline:
 914

915

- 916 **Coordinate centering:** Atomic coordinates are centered by subtracting the center of mass:
 917
$$\mathbf{r}_i \leftarrow \mathbf{r}_i - \frac{1}{|m|} \sum_j \mathbf{r}_j$$

918
919
920
921
922
923
924
925
926
927
928
929
930
931
932
933
934
935
936
937
938
939
940
941
942
943
944
945
946
947
948
949
950
951
952
953
954
955
956
957
958
959
960
961
962
963
964
965
966
967
968
969
970
971
Table 5: Training hyperparameters used for all TransIP experiments.

| Hyperparameter | Value |
|----------------------------------|-----------------------------------|
| <i>Optimization:</i> | |
| Optimizer | AdamW |
| Learning rate | 5×10^{-4} |
| Weight decay | 1×10^{-3} |
| Gradient clip norm | 200 |
| <i>Learning rate schedule:</i> | |
| Scheduler type | Cosine |
| Warmup fraction | 0.01 |
| Min LR factor | 0.01 |
| <i>Loss weights:</i> | |
| Energy (λ_E) | 5 |
| Forces (λ_F) | 15 |
| Equivariance (λ_{leg}) | 5 (selected from {1, 5, 10, 100}) |

- **Equivariance pairs:** For training with learned equivariance, we create pairs $(m, \phi(g)(m))$ where g is sampled uniformly from $\text{SO}(3)$ per molecule.

A.4 EVALUATION METRICS

We evaluate model performance using the following metrics:

Force Mean Absolute Error (MAE):

$$\text{Force MAE} = \frac{1}{3|m|} \sum_{i=1}^N \sum_{\alpha \in \{x, y, z\}} |\mathbf{F}_{i,\alpha} - \mathbf{F}_{i,\alpha}^*| \quad (\text{meV/}\text{\AA}) \quad (8)$$

Force Cosine Similarity:

$$\text{Force CosSim} = \frac{1}{|m|} \sum_{i=1}^{|m|} \frac{\mathbf{F}_i \cdot \mathbf{F}_i^*}{\|\mathbf{F}_i\| \|\mathbf{F}_i^*\|} \quad (9)$$

Energy per Atom MAE:

$$\text{Energy/atom MAE} = \frac{1}{|m|} |E - E^*| \quad (\text{meV/atom}) \quad (10)$$

Total Energy MAE:

$$\text{Total Energy MAE} = |E - E^*| \quad (\text{meV}) \quad (11)$$

where \mathbf{F} and E denote predicted forces and energies, \mathbf{F}^* and E^* are ground truth values, and $|m|$ is the total number of atoms. For energies, we use referenced targets following [Levine et al. \(2025\)](#).

A.5 COMPUTATIONAL RESOURCES

- 5-epoch experiments: 8 NVIDIA 80GB GPUs
- 80-epoch experiments: 64 NVIDIA 80GB GPUs

A.6 VALIDATION SPLITS

For 5-epoch runs, we evaluate on domain-specific validation subsets sampled from the OMol25 validation (Val-Comp) dataset:

- Metal complexes: 20,000 samples

- Electrolytes: 20,000 samples
- Biomolecules: 20,000 samples
- SPICE: 9,630 samples (complete subset)
- Neutral organics: 20,000 samples (including ANI2x, OrbNet-Denali, GEOM, Trans1x, RGD)
- Reactivity: 20,000 samples
- Full validation set: 20,000 samples.

We use the full (2M) Val Comp dataset to evaluate TransIP and TransAug in Table 1.

B ADDITIONAL RESULTS

B.1 OPEN CATALYST BENCHMARK

We also evaluate our method on the Open Catalyst 2020 (OC20) benchmark (Chanussot et al., 2021), a large-scale dataset for modeling catalyst-adsorbate interactions. We train on the 2M subset from the Structure-to-Energy-and-Forces (S2EF) task, and for validation, we selected 20,000 samples from each validation split: `val_id` (in-distribution) and `val_ood` (out-of-distribution). We use the small version of TransIP and TransAug with the same hyperparameters in Tables 3 and 5, trained for 30000 steps. Our results are presented in Table 6. Our results show that TransIP consistently outperforms TransAug on energy metrics on both in-distribution and out-of-distribution splits, and matches TransAug on force MAE.

| Model | val_id | | val_ood | |
|------------|----------|----------|----------|----------|
| | Energy ↓ | Forces ↓ | Energy ↓ | Forces ↓ |
| TransAug-S | 56 | 82 | 72 | 95 |
| TransIP-S | 45 | 82 | 55 | 95 |

Table 6: OC20 S2EF energy and force MAE on `val_id` and `val_ood` splits.

B.2 OMOL25 SPLITS

In this section, we include additional dataset scaling results on OMol25 splits for TransIP and TransAug.

| Model | Epochs | SPICE | | Reactivity | |
|------------|--------|----------|----------|------------|----------|
| | | Energy ↓ | Forces ↓ | Energy ↓ | Forces ↓ |
| TransAug-S | 5 | 11.5 | 151.3 | 23.0 | 179.7 |
| TransIP-S | 5 | 8.7 | 121.8 | 17.8 | 136.4 |

Table 7: Val-Comp energy and force MAE for SPICE and Reactivity splits.

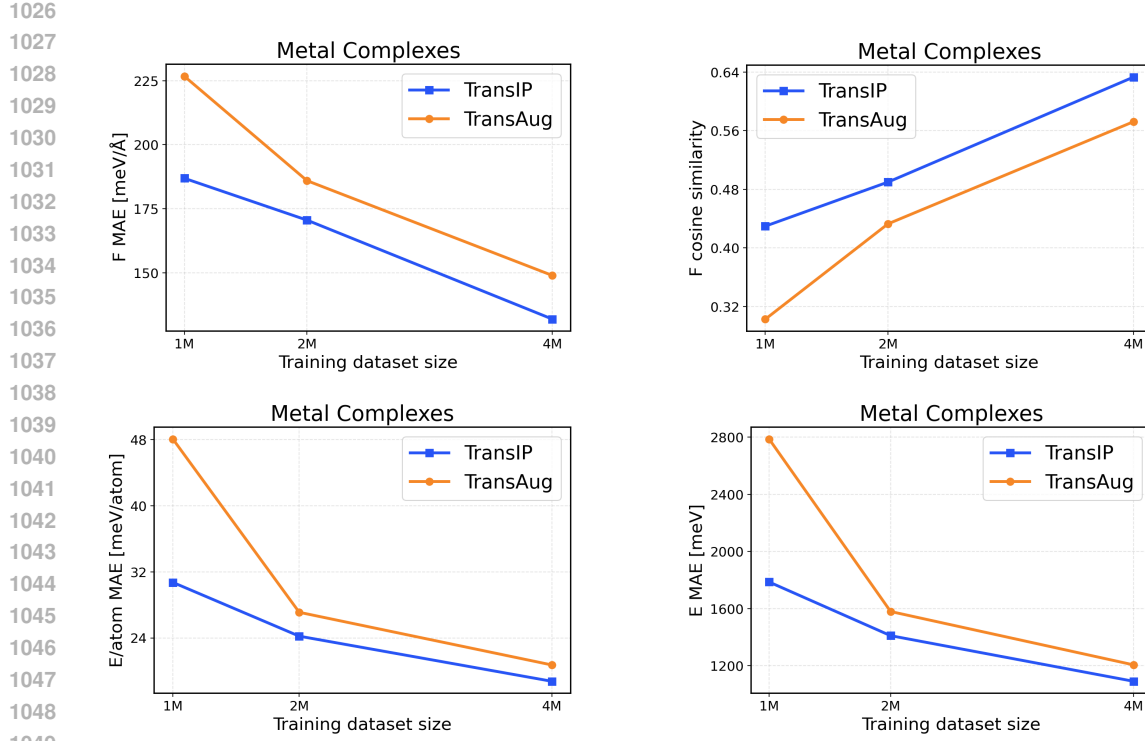


Figure 6: Metal Complexes scaling across training dataset sizes (1M / 2M / 4M). The top row presents force metrics, while the bottom row displays energy metrics.

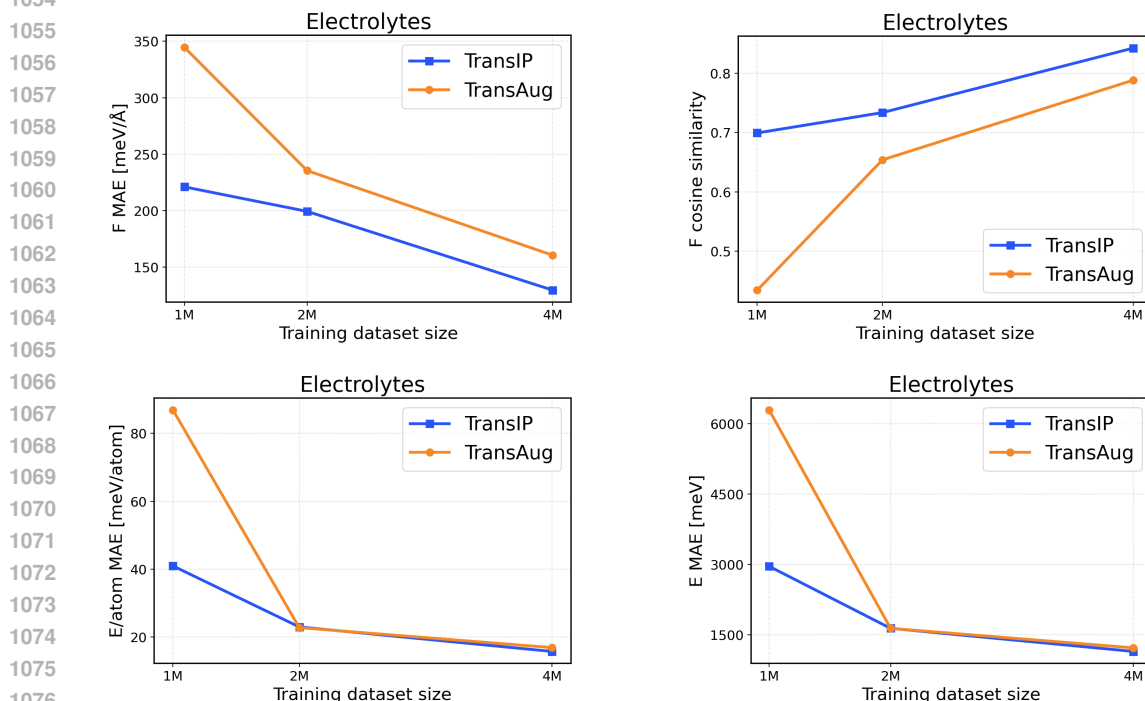
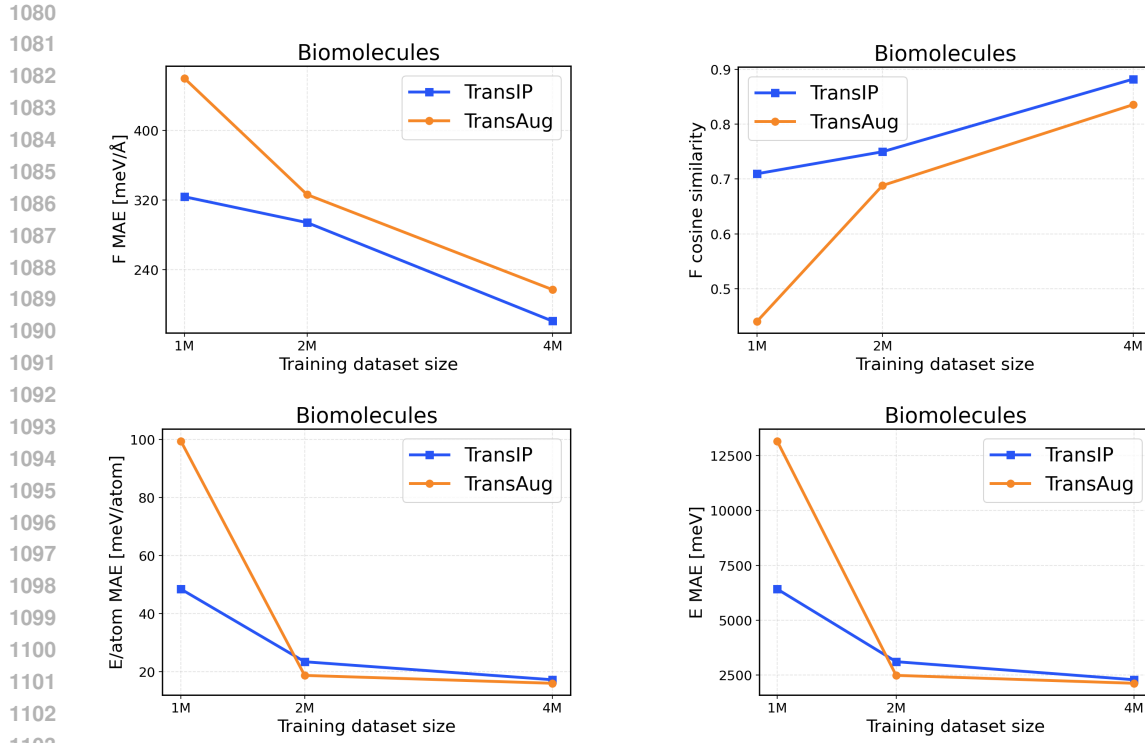


Figure 7: Electrolytes scaling across training dataset sizes (1M / 2M / 4M). The top row presents force metrics, while the bottom row displays energy metrics.



1104
1105
1106
1107
1108
1109
1110
1111
1112
1113
1114
1115
1116
1117
1118
1119
1120
1121
1122
1123
1124
1125
1126
1127
1128
1129
1130
1131
1132
1133

Figure 8: Biomolecules scaling across training dataset sizes (1M / 2M / 4M). The top row presents force metrics, while the bottom row displays energy metrics.

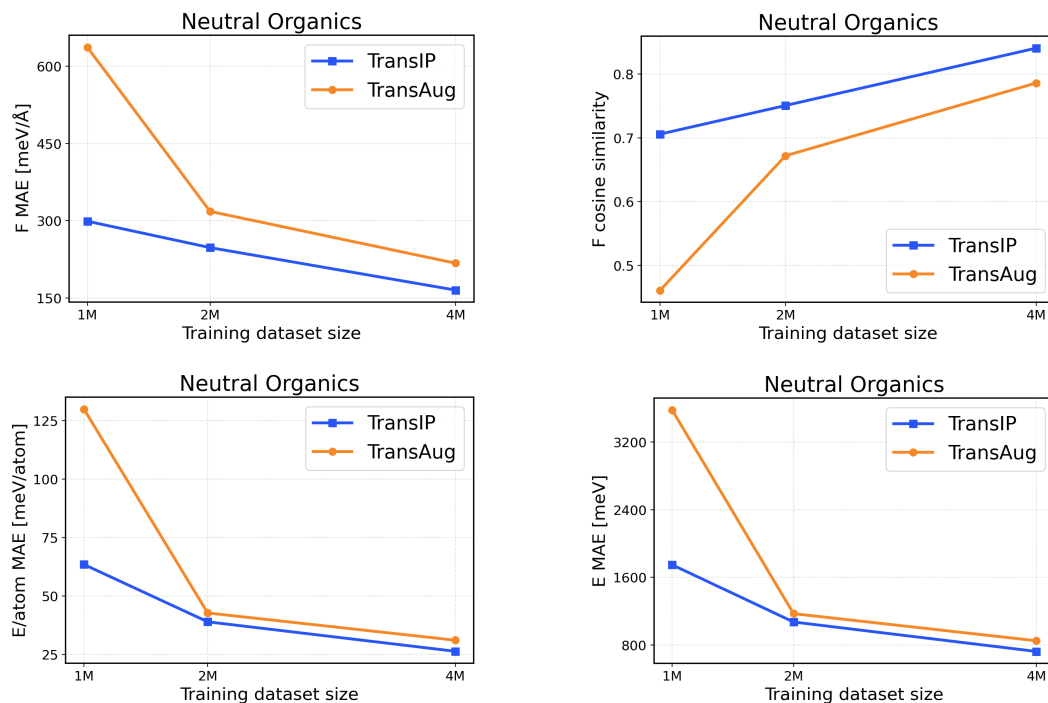


Figure 9: Neutral Organics scaling across training dataset sizes (1M / 2M / 4M). The top row presents force metrics, while the bottom row displays energy metrics.

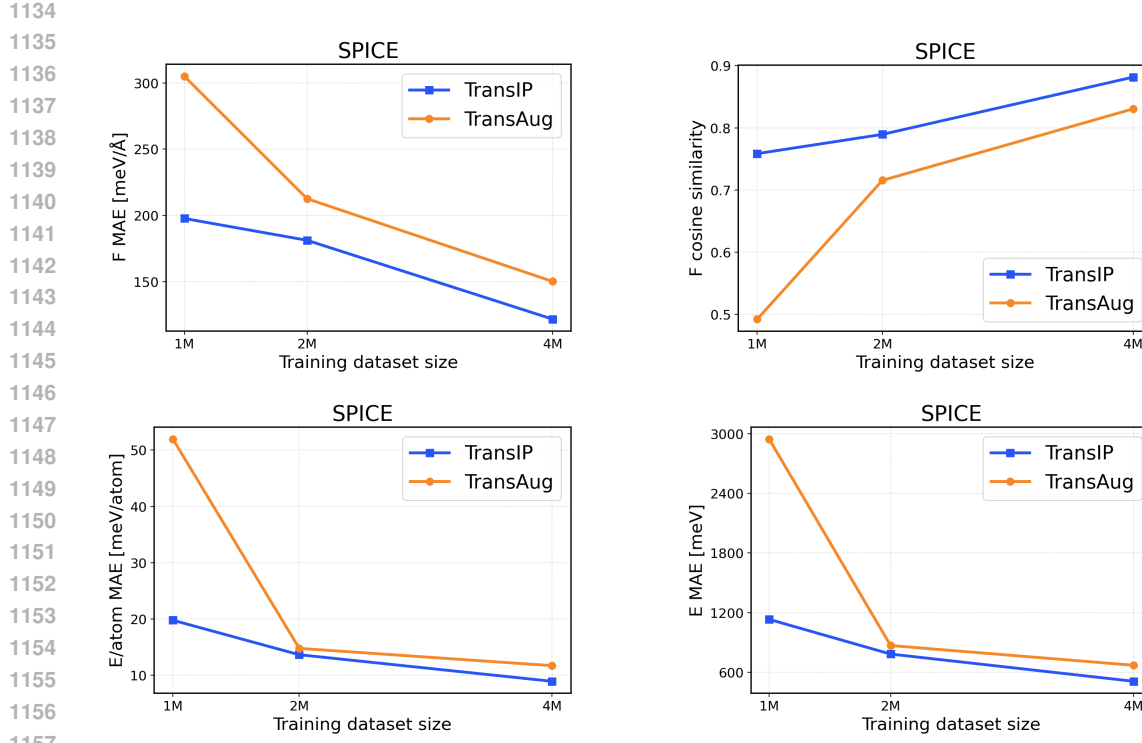


Figure 10: SPICE scaling across training dataset sizes (1M / 2M / 4M). The top row presents force metrics, while the bottom row displays energy metrics.

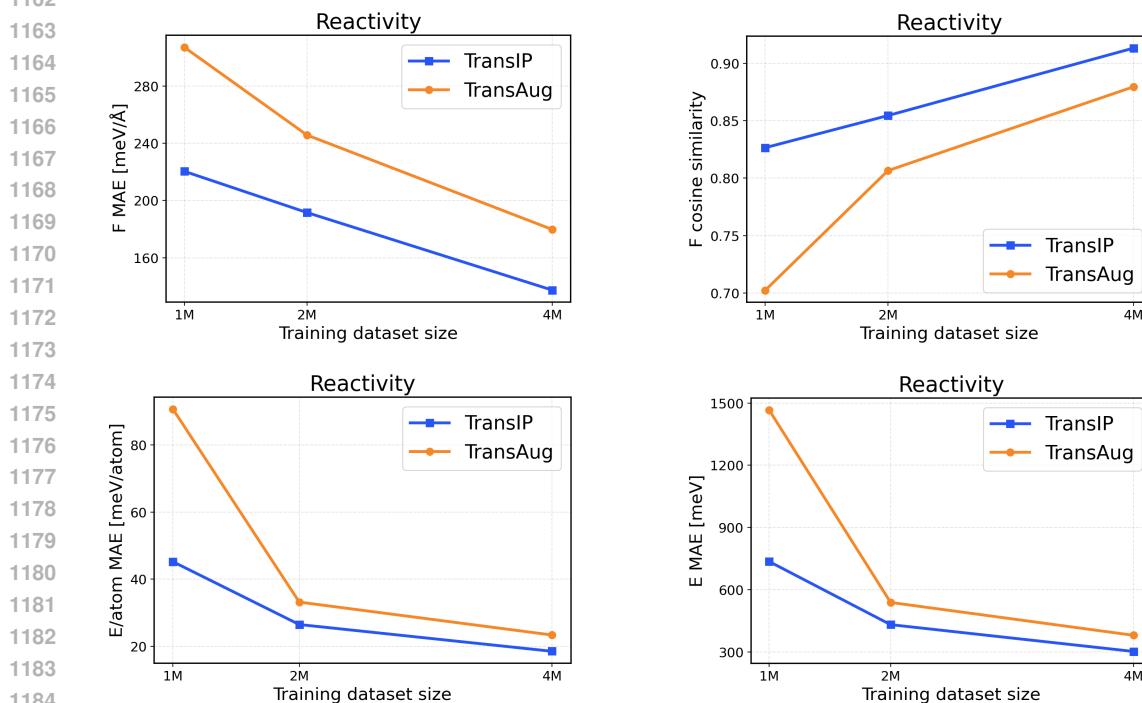


Figure 11: Reactivity scaling across training dataset sizes (1M / 2M / 4M). The top row presents force metrics, while the bottom row displays energy metrics.